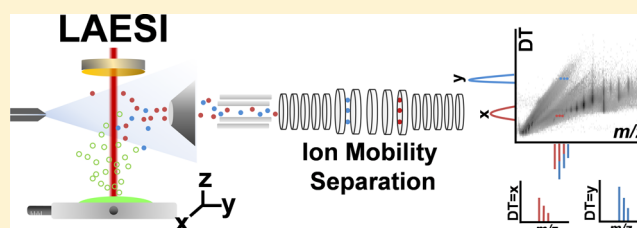# High-Throughput Cell and Tissue Analysis with Enhanced Molecular Coverage by Laser Ablation Electrospray Ionization Mass Spectrometry Using Ion Mobility Separation

Bindesh Shrestha and Akos Vertes*

Department of Chemistry, W. M. Keck Institute for Proteomics Technology and Applications, George Washington University, Washington, District of Columbia 20052, United States

Ⓢ *Supporting Information*

ABSTRACT: Ambient ionization methods, such as laser ablation electrospray ionization (LAESI), facilitate the direct analysis of unperturbed cells and tissues in their native states. However, the lack of a separation step in these ionization techniques results in limited molecular coverage due to interferences, ion suppression effects, and the lack of ability to differentiate between structural isomers and isobaric species. In this contribution, LAESI mass spectrometry (MS) coupled with ion mobility separation (IMS) is utilized for the direct

analysis of protein mixtures, megakaryoblast cell pellets, mouse brain sections, and *Arabidopsis thaliana* leaves. We demonstrate that the collision cross sections of ions generated by LAESI are similar to the ones obtained by ESI. In various applications, LAESI-IMS-MS allows for the high-throughput separation and mass spectrometric detection of biomolecules on the millisecond time scale with enhanced molecular coverage. For example, direct analysis of mouse brain tissue without IMS had yielded ∼300 ionic species, whereas with IMS over 1 100 different ions were detected. Differentiating between ions of similar mass-to-charge ratios with dissimilar drift times in complex biological samples removes some systematic distortions in isotope distribution patterns and improves the fidelity of molecular identification. Coupling IMS with LAESI-MS also expands the dynamic range by increasing the signal-to-noise ratio due to the separation of isobaric or other interfering ionic species. We have also shown that identification of potential biomarkers by LAESI can be enhanced by using the drift times of individual ions as an additional parameter in supervised orthogonal projections to latent structures discriminant analysis. Comparative analysis of drift time versus mass-to-charge ratio plots was performed for similar tissue samples to pinpoint significant metabolic differences.

Ambient ionization techniques are gaining ground for the nontargeted direct analysis of cells and tissues by mass spectrometry (MS).[1−3] These methods allow rapid sampling and ionization at atmospheric pressure without a need for extensive sample preparation.[4−6] Because of the inherent complexity of biological systems, chemical characterization limited to MS without a separation step often does not differentiate between structural isomers and other isobaric species and regularly lumps conformers together. Direct ionization methods cannot use conventional chromatographic separation methods because ion production takes place immediately after sampling.

In ion mobility separation (IMS), chemical species are rapidly distinguished (within ∼10 ms) according to their collision cross sections (size and shape) through their interaction with the buffer gas. While drifting through a cell filled with an inert gas under electric field, ions of same m/z value with a smaller collision cross section drift faster than ions with larger cross sections, providing information on their physical size.

Introduced about a half a century ago as plasma chromatography, IMS has been used in conjunction with an array of ionization sources.[7,8] Radioactive sources, such as

electron-emitting ^{63}Ni, are commonly used for their stability and reliability but are being discouraged due to the regulatory and maintenance costs.[8] Recently many nonradioactive ionization sources, such as corona discharge ionization,[9] photoionization via photodischarge lamps or lasers,[10−12] surface ionization,[13] electrospray ionization,[14,15] glow discharge ionization,[16] etc., have been used with IMS analyzers.

Ion mobility spectrometry with a Faraday cup detector has found broad use in military and security applications for detecting chemical warfare agents, explosives, toxic industrial wastes, and narcotics.[17] By coupling IMS with a mass spectrometer, molecules can be resolved based on drift time (DT) and m/z. IMS adds the ability to extend the dynamic range of mass spectrometric analysis by separating isomeric and isobaric peaks in a sample. In the past decade, IMS-MS has evolved into a powerful tool for evaluating structures of biomolecules in the gas-phase.[18] IMS-MS has been utilized for the analysis of protein conformers,[19] structural isomers of peptides,[20] chiral separation of a racemic mixture of small

metabolites,[21] polymers,[22] etc. Ion mobility separation increases peak capacity in MS, separates isobaric ions with similar m/z values, reduces chemical noise, and provides information on the collision cross sections of ions.

Various ambient ion sources have been coupled with IMS alone or IMS-MS for the analysis of drugs and proteins by desorption electrospray ionization (DESI),[23,24] pharmaceuticals in direct analysis in real time (DART),[25] pharmaceutical solutions in paper spray,[26] and antimalarial drugs in laser ablation/desorption electrospray ionization (LADESI).[27]

Laser ablation electrospray ionization (LAESI) is an ambient ionization method that has been utilized for the *in situ* analysis of tissues, single plant cells, and subcellular components.[3,28,29] Several ambient ionization techniques using laser sampling and subsequent ionization by electrospray, such as electrospray-assisted laser desorption/ionization (ELDI),[30] infrared laser-assisted desorption electrospray ionization (IR LADESI),[31] infrared laser desorption electrospray ionization (IR-LDESI),[32] laser electrospray mass spectrometry (LEMS),[33] laser desorption spray postionization mass spectrometry (LDSPI-MS),[34] matrix-assisted laser desorption electrospray ionization (MAL-DESI),[35,36] laser ablation atmospheric pressure photoionization (LAAPPI),[37] have been introduced. In all of the ionization methods, solid or liquid samples are desorbed or ablated at atmospheric pressure yielding mostly neutrals, which are intercepted and ionized by an electrospray plume. The combination of LAESI with IMS is feasible because the sampling rates and separation times of the two methods, respectively, are comparable.

In this contribution, we describe the combination of LAESI for direct ionization of molecules in cell pellets and tissues, with separation using IMS and detection by MS. We expect to increase the coverage of the metabolome and lipidome of biological samples by introducing IMS as a separation step. The capabilities of enhanced analysis by LAESI-IMS-MS are illustrated by selected applications of this new technique for the analysis of megakaryoblast cell pellets, mouse brain tissue sections, and *Arabidopsis thaliana* leaves.

■ MATERIALS AND METHODS

Laser Ablation Electrospray Ionization. The LAESI technique with conventional optics for laser pulse delivery has been described previously.[3] Briefly, 5 ns pulses of the idler beam from an optical parametric oscillator (OPO) tuned to the 2940 nm wavelength (Opolette 100, Opotek, Carlsbad, CA) were steered by three gold-coated mirrors (PF10-03-M01, Thorlabs, Newton, NJ) to a 75 mm focal length ZnSe plano-convex lens (Infrared Optical Products, Farmingdale, NY). The beam was focused on the sample surface, and the produced ablation plume was intercepted by an electrospray of 50% methanol solution with 0.1% acetic acid (v/v) (Fluka, Seelze, Germany). The solution was delivered by a precision syringe pump (Pump 11 Plus, Harvard Apparatus, Holliston, MA) at a flow rate of 400 nL/min through a stainless steel emitter (MT320-50-5-5, New Objective, Woburn, MA) held at +3300 V by a regulated power supply (PS350, Stanford Research Systems, Sunnyvale, CA). A homemade Peltier cooling stage, described earlier,[38] kept the degradation-prone samples, e.g., brain tissue sections, below the freezing temperature (at −5 °C) during the analysis to minimize biochemical changes and dehydration.

Ion Mobility Separation. The LAESI-generated ions were sampled by a high performance quadrupole time-of-flight mass

spectrometer with a traveling-wave (T-wave) IMS system (Synapt G2S, Waters, Milford, MA). The MS studies were conducted in all three modes of the time-of-flight system: sensitivity (V-mode), resolution (V-mode), and high resolution (W-mode). The principles and operation of the T-wave IMS coupled with electrospray ionization were discussed elsewhere.[39] In T-wave IMS, a periodic electric field sweeps in the direction of the movement of ions as they travel through the mobility cell. Because of scattering on the background gas atoms, the ions are separated according to their collision cross section. The IMS cell was operated with constant wave heights selected between 14 and 40 V, and the wave velocity was fixed between 650 and 2000 m/s. Nitrogen was supplied as the drift gas at a flow rate of 90 mL/min and a pressure of 3.25 mbar in the mobility cell. In the Synapt G2S, there are two additional traveling wave ion guides flanking the IMS cell. The first one (Trap = T1) traps and releases ions to the IMS, whereas the second one (Transfer = T2) transfers the ions to the time-of-flight mass spectrometer for detection (see Figure 1). Ions in a
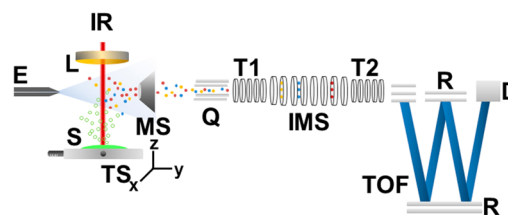

Figure 1. Graphical representation of laser ablation electrospray (LAESI) ion mobility separation (IMS) mass spectrometry (MS) is presented. Mid infrared laser (IR) is focused through an antireflection-coated ZnSe lens (L) to a sample (S) placed on a three-axis translation stage (TS). The ablated neutral plume particulates (hollow dots) are postionized by electrospray produced through an emitter (E). The postionized ions (solid dots) are sampled inside the mass spectrometer orifice (O). The collected ions are separated based on their mobility by traveling wave ion mobility separation (IMS) and detected by a detector (D) with a high resolution time-of-flight (TOF) system with a dual-stage reflectron (R).

selected mass-to-charge ratio range (e.g., $\Delta m/z \sim 1$ window), defined by the quadrupole (Q), can be subjected to collision-induced dissociation (CID) both in the trap and the transfer cells. The quadrupole entrance cell installed in front of the ion mobility cell was flushed with helium at a flow rate of 180 mL/min. The trap and transfer cells were supplied with argon at a flow rate of 2 mL/min. The trapping release time from T1 was 200 μs, whereas the IMS wave delay was 450 μs. A schematic representation of the entire LAESI-IMS-MS is shown in Figure 1.

Samples. Lysozyme from chicken egg white (L6876, ≥90% pure lyophilized powder), myoglobin from equine heart (M1882, ≥90% pure lyophilized powder), and ubiquitin from bovine erythrocytes (U6253, ≥98% pure lyophilized powder) were obtained from Sigma-Aldrich (St. Louis, MO) and used without further purification. Glu-1-Fibrinopeptide B (Glu-Fib) peptide standard was obtained from Protea Biosciences Group, Inc. (Morgantown, WV). Human megakaryoblast cell lines (MEG-01, ATCC no. CRL-2021, Manassas, VA), established from a chronic myeloid leukemia patient, were grown in RPMI-1640 medium (ATCC no. 30-2001, Manassas, VA) with 10% fetal bovine serum supplemented with 1% penicillin and streptomycin antibiotics.[40] Pellets were produced by centrifu-

gation of the washed cells for 10 min at 300 rcf in 2-mL plastic vials.

For brain tissue samples, healthy mice (C57Bl/10, Jackson Laboratory, Bar Harbor, ME) were euthanized, and their brains were extracted and flash frozen. Coronal sections from near the bregma were excised, and the frozen tissue was directly analyzed. The experimental procedure for the animals complied with the principles set forth in the "Guide for the Care and Use of Laboratory Animals" prepared by the Committee on Care and Use of Laboratory Animals of the Institute of Laboratory Resources, National Research Council.

Wild type *Arabidopsis thaliana* var. Columbia plants were grown for 4−6 weeks in a growth chamber alternating between 16 h light (22 °C, 120 μmol m^{-2} s^{-1}) and 8 h dark (20 °C) periods and maintaining 70% humidity. For the LAESI-IMS-MS experiments, leaves were obtained from healthy plants.

Data Processing. Raw LAESI-IMS-MS data sets can be as large as 1−2 GB. Mass spectra were collected and initially processed by the MassLynx 4.1 software (Waters, Milford, MA). Ions were putatively classified as metabolites, lipids, and peptides based on the combination of drift time and accurate monoisotopic mass measurements, isotope distribution patterns, chemical databases/literature search, and, in some cases identified based on tandem MS. The theoretical monoisotopic masses were calculated using the NIST Isotope Calculator package (ISOFORM, version 1.02). Metabolomic and lipid databases, METLIN (http://metlin.scripps.edu, last accessed December 2, 2013) and LIPID MAPS (http://lipidmaps.org, last accessed December 2, 2013), were searched for species within a 10 ppm accuracy window of the experimental m/z values. After Pareto scaling, orthogonal projections to latent structures discriminant analysis (OPLS-DA) was performed in the Extended Statistics (XS) module of the MarkerLynx application manager (Waters, Milford, MA) that utilizes the EZinfo software (version 2.0.0.0, Umetrics AB, Sweden). The DriftScope 2.4 module (Waters, Milford, MA) was used for reviewing and visualizing ion intensities as a function of drift time and m/z (DT vs m/z plots). The HDMS Compare 1.0 software (Waters, Milford, MA) enabled the comparison of DT vs m/z data sets. Multiply charged ion peaks were deconvoluted using the MaxEnt 1 software (Waters, Milford, MA) using the maximum entropy method.

Collision Cross-Section Calculations. A multistep protocol to produce the calibration curve connecting the measured drift times, t_D, in a traveling wave device with the ion collision cross sections has recently been described.[41] The corrected drift time, t_D', was defined as $t_D' = t_D - C (m/z)^{1/2}/1000$, where the drift time values were substituted in milliseconds, and the instrument specific constant, C, also known as the instrument setting-specific enhanced duty cycle (EDC) delay coefficient, for the Synapt G2S was found to be $C = 1.41$ (MassLynx 4.1, Waters, Co.). This C constant characterizes the time spent by the ions between the end of the drift tube and the mass analyzer. The collision cross section in a traveling wave IMS is a nonlinear function of the corrected drift time, $\Omega = A(z_e)/\sqrt{\mu}t_D'^X$, where z_e is the charge of the studied ion, μ is the reduced mass of the ion and the argon collision gas atom, and A and X are the calibration parameters. Estimated values for A and X were obtained by plotting the logarithm of the modified collision cross section using equation $\ln \Omega' = \ln((\Omega\sqrt{\mu})/(z_e)) = X \ln t_D' + \ln A$, and performing linear regression provided estimated values for $X = 0.642 \pm 0.010$ and $\ln A = 7.384 \pm 0.005$ with an $R^2 = 0.998$. Introducing

the transformed corrected drift time, $t_D'' = (z_e)/\sqrt{\mu}t_D'^X$, a linearized form of the collision cross section, $\Omega = At_D''$, was plotted (see Figure S1c in the Supporting Information).

The range of measured t_D in this study was in the 0−4 ms range. This range was determined by the wave velocity that in turn was linked to the repetition rate of the pusher voltage for the time-of-flight system. Selecting a narrower m/z range enabled the selection of the slower wave velocity and longer t_D.

■ RESULTS

LAESI Combined with IMS-MS. The commercial ESI source of the Synapt G2S IMS-MS system was replaced by the home-built LAESI source, and the geometry, voltage, and laser ablation parameters (pulse energy and focusing) were optimized using lyophilized Glu-Fib standard in aqueous solution. To test the utility of LAESI-IMS-MS for larger molecules and their close to equimolar mixtures, purified protein samples that included lysozyme, myoglobin, and ubiquitin dissolved in 50% aqueous methanol solution were directly analyzed. Control experiments were performed with the electrospray running without laser pulses. In Figure S1a of the Supporting Information, a two-dimensional DT vs m/z plot and the corresponding mass spectrum for 650 × 10^{-6} M aqueous lysozyme solution are shown. Both the DT vs m/z plot and the mass spectrum display multiply charged lysozyme ions from charge states 6+ to 11+. The charge states of the ions were determined from the spacing of the isotope peaks. For example the peaks at nominal m/z 2385, in the inset of the bottom panel, corresponded to [M + 6H]$^{6+}$. The circled portion of the DT vs m/z plot highlights two areas of high intensity for the [M + 7H]$^{7+}$ species. The ion intensities of [M + 7H]$^{7+}$ as a function of drift time displays two partially resolved peaks, at DT = 0.54 and 0.73 ms, respectively, suggesting the presence of two relatively stable conformations for the 7+ charge state[39] with significantly different collision cross sections. The ability to detect distinct conformations of a protein species produced by laser ablation of a solution sample holds the possibility of exploring molecular conformations in tissue samples.[42]

Figure S1b of the Supporting Information shows a DT vs m/z plot for a mixture of lysozyme (115 μM), myoglobin (100 μM), and ubiquitin (130 μM). Multiply charged proteins species are highlighted in the DT vs m/z plot. Dissolving myoglobin in the 50% methanol disrupts the noncovalent interactions between the protein and the prosthetic group. The resulting mass spectrum consists of multiply charged holo- and apomyoglobin ions and an additional charged species at m/z 616 corresponding to heme B.[43] The drift time distribution is shown on the left, whereas a mass spectrum integrated over the myoglobin-related ions is displayed on the top, with an inset of the deconvoluted spectrum recovering the correct molecular weight, 16 951 Da, of equine heart apomyoglobin.[44]

Determining the collision cross sections in a traveling wave IMS system requires extensive calibration with ions of known cross sections following the procedure described in the Experimental Section. Literature data for the collision cross-section, Ω, values of apomyoglobin ions in charge states between 10+ and 18+ were used to establish a correlation with drift times. The Ω values for lysozyme[45] and ubiquitin[46] were obtained from the related literature and for apomyoglobin from the Clemmer Group Cross Section Database at http://www.indiana.edu/~clemmer (last accessed on December 12, 2013).[47] Regression analysis showed a linear relationship for
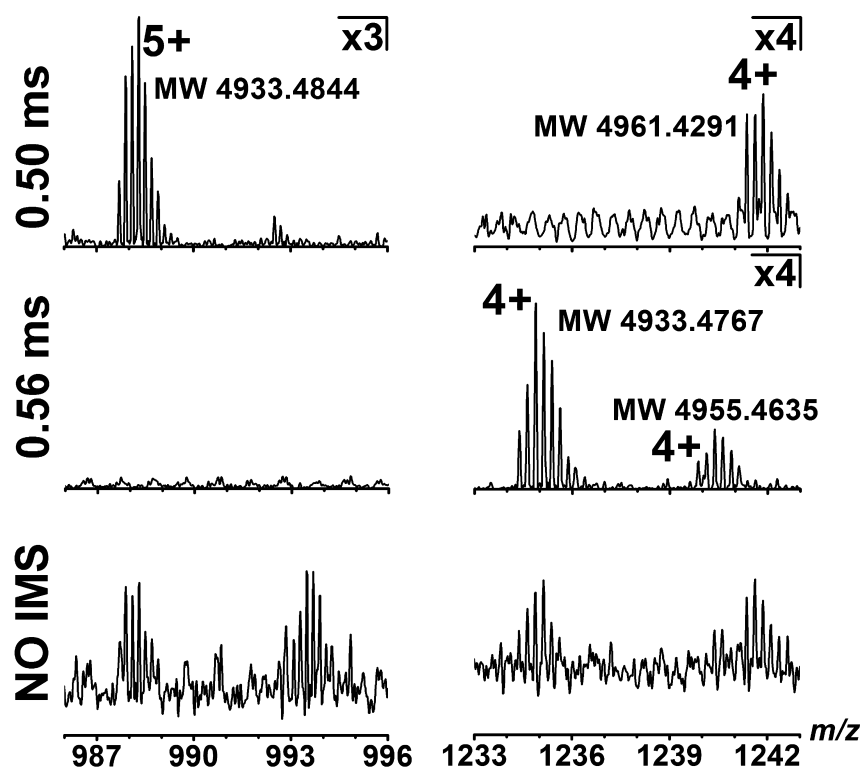
Figure 2. Comparing selected regions of the LAESI mass spectra from a human megakaryoblast (MEG-01) cell pellet without and with IMS reveal significantly reduced spectral interferences and an improved signal-to-noise ratio for the latter.

the collision cross section as a function of the transformed corrected drift time for multiply protonated apomyoglobin species with an $R^2 = 0.994$. For verification of its accuracy, this calibration curve was used to empirically determine the collision cross sections for lysozyme and ubiquitin ions analyzed in the same run. The estimated collision cross sections, reported in Table S1 of the Supporting Information, were within 0−4% of the values reported for electrospray ionization from a solvent containing 49% aqueous acetonitrile with 2% acetic acid. Denatured ubiquitin ions produced from such a nonphysiological solvents are known to exhibit a significantly larger collision cross sections than the ones produced from pseudonative solvents with higher water content.[48] Recovering the values of collision cross sections determined by electrospray ionization under denaturing conditions in a LAESI experiment that utilizes a denaturing spray solution (50% methanol solution with 0.1% acetic acid) indicates that the conformations of protein ions, produced by these two techniques, can be similar. This finding is consistent with our earlier studies of LAESI-generated ions that have shown their internal energies being indistinguishable from the electrospray generated counterparts.[49]

Signal Enhancement in Cell Pellet Analysis. Successful direct analysis of cells and pellets from cell cultures entails distinguishing the signal produced by the chemical species arising from the cells themselves from the interfering peaks corresponding to the media and buffers used to maintain them.[50] For example, the PBS buffer, used to wash the cells, often produces sodium chloride cluster ions that interfere with the detection of phospholipids.[51]

LAESI-IMS-MS can help to separate the buffer-related background ions, as well as the ions generated by the electrospray solvent, from the sample-related ions. Direct analysis of human megakaryoblast cell pellets by LAESI-IMS-MS resulted in DT vs m/z plots with numerous peaks corresponding to metabolites and lipids (not shown). In order to discern the origin of ions, the ions found in the electrospray background and those generated by LAESI analysis of the buffer were compared with the ions obtained from cell pellets. The bottom panel in Figure 2 depicts zoomed segments of a mass spectrum, in the m/z 986−996 and m/z 1233−1243 ranges, averaged over the entire drift time distribution, i.e., without IMS. These traces indicate low signal-to-noise ratio and appear to be affected by interferences. In comparison, spectra with IMS at specific drift times, 0.50 ms (top panel) and 0.56 ms (middle panel), exhibit significantly improved signal for the m/z 986−996 and m/z 1233−1243 ranges, respectively. For example, the peaks for multiply charged ions at m/z 988 are present in the mass spectrum without IMS (bottom panel) but with a poor signal-to-noise ratio (S/N). In the mass spectrum collected at drift time 0.50 ms (top panel), the S/N for these ions is improved by at least an order of magnitude. The IMS also enabled the reliable determination of the charge state as 5+ for these ions, and the calculation of the corresponding molecular mass as 4933.5 Da. The mass spectrum collected at drift time 0.56 ms shows the same molecule in the 4+ charge state with a calculated mass of 4933.5 Da. The difference between the masses calculated from the 5+ and 4+ ions is only 7.7 mDa or 1.6 ppm.

In addition to improving the S/N ratio, IMS also reduced the interferences between overlapping peaks. For example, the group of peaks at nominal m/z 1242 without IMS seemingly corresponded to the isotope peaks of a single quadruply charged ion. Studied with IMS at drift times of 0.50 and 0.56 ms, this feature was resolved into two distinct 4+ ions with calculated masses of 4961.4 and 4955.5 Da, respectively. These

examples demonstrate that LAESI-IMS-MS can reduce chemical interferences in the mass spectra as well as improve the fidelity of isotope distribution patterns by separating isobaric ions in complex samples.

Improved Molecular Coverage for Mouse Brain Sections. Direct LAESI-IMS-MS was performed on a coronal section adjacent to the bregma of a healthy mouse brain. The corresponding DT vs m/z plot displays a large set of data with specific regions primarily corresponding to metabolites, lipids, polypeptides and proteins (see the circled areas in the top panel of Figure 3). The overall number of detected ionic species

Figure 3. DT vs m/z plot produced by LAESI-IMS-MS from a coronal section of mouse brain is shown with highlighted regions corresponding to small metabolites, lipids, polypeptides, and proteins. Mass spectra extracted from the highlighted regions show enhanced signal for lipids (bottom left panel) and polypeptides (bottom right panel), including a species with a molecular mass very close to thymosin β4 (see inset in bottom right panel).

exceeded 1 100 that compared favorably with the ~300 peaks in earlier LAESI-MS studies on mouse brain tissue without IMS.[38] This enhanced molecular coverage manifested itself in finding a larger number of ions in previously identified compound groups, i.e., small metabolites and lipids, as well as observing previously hidden components, e.g., proteins and polypeptides.

Because of their relatively small sizes and low molecular weights, ions classified as metabolites were found at short drift times and low m/z values. Lipids, because of their larger collision cross section, had longer drift times than metabolites and peptides with similar m/z.[52] Multiply charged proteins and polypeptides were found in the same m/z range, where the stronger signal for the proteins could mask the polypeptide peaks. However, multiply charged proteins exhibited slightly longer drift times than polypeptides due to their larger size. These observations only serve as general guidance for the

classification of these compound groups in the DT vs m/z plot. In the relatively few cases when tandem MS measurements are available from current or past LAESI-MS of the mouse brain tissue, we have identified the ions. For example, the m/z 760.586 ion had been identified by tandem MS as protonated PC(34:1).[38]

The bottom panels in Figure 3 present mass spectra obtained from the highlighted lipid (left) and polypeptide (right) regions in the DT vs m/z plot. Selection of different regions results in profoundly different mass spectra with enhanced isotope distribution patterns and a discernible presence of numerous low intensity ions that have been obscured in the drift time-averaged mass spectra because of the presence of adjacent multiply charged protein species. For example, the deconvolution of the ions in the m/z 993 to 995 region in the bottom right panel yielded a molecular mass of 4961.4 Da (see the inset in bottom right panel of Figure 3), a value very similar to that of thymosin β4, a ubiquitous multifunction polypeptide that is associated with, e.g., G-actin sequestration and brain tissue protection.[53]

The mass spectrum corresponding to the area marked as "Proteins" in the DT vs m/z plot is shown in Figure S2 of the Supporting Information. Two series of multiply charged species are apparent in the m/z 850−1550 region (see the peaks marked by ∗ and γ). Deconvolution of these peaks yields two proteins with molecular masses of 14.9 kDa (∗) and 15.6 (γ) kDa (see the inset in Figure S2 of the Supporting Information). Averaging of mass spectra from selected regions of the DT vs m/z plot is beneficial for identifying low abundance chemical species and thus enhances the simultaneous analysis of metabolites, lipids, polypeptides, and proteins.

Enhanced Comparative Analysis of *A. thaliana* Leaf Segments. Two DT vs m/z plots from the analysis of the edge and midvein sections of an *A. thaliana* leaf are shown in the top and bottom of Figure 4, respectively, with hundreds of peaks in each. Comparing such a large number of spectral features in similar biological samples is often difficult, due to the variations within each sample type that can obscure the small differences between them. Multivariate statistical analysis tools, e.g., orthogonal projections to latent structures-discriminant analysis (OPLS-DA) had been helpful in exploring the differences between two sets of similar mass spectra generated by LAESI-MS without IMS.[54,29,55]

In order to assess the utility of this technique to the more complex LAESI-IMS-MS data sets, S-plots connecting the correlation with the covariance for the predictive components were generated for the edge and midvein sections of the leaves (see Figure S3 in the Supporting Information). Positive correlation values represent ions from the edge of the leaves, whereas negative values indicate ions from their midvein. Initially a global S-plot is produced for all DT values included to find the most prominent differences between the two data sets (see Figure S3a in the Supporting Information). This analysis identifies sucrose with the largest absolute covariance and correlation values as being significantly more abundant in the spectra from the midvein region.

To accentuate peak intensity differences within a group of similar compounds, e.g., small metabolites or lipids, S-plots can be generated for selected DT values. For example, Figure S3b of the Supporting Information shows the S-plot for DT = 0.52 ms, a characteristic value for small metabolites. Inspecting the point corresponding to sucrose indicates that within this subset of the data, its covariance has increased from 0.21 to 0.56, i.e.,
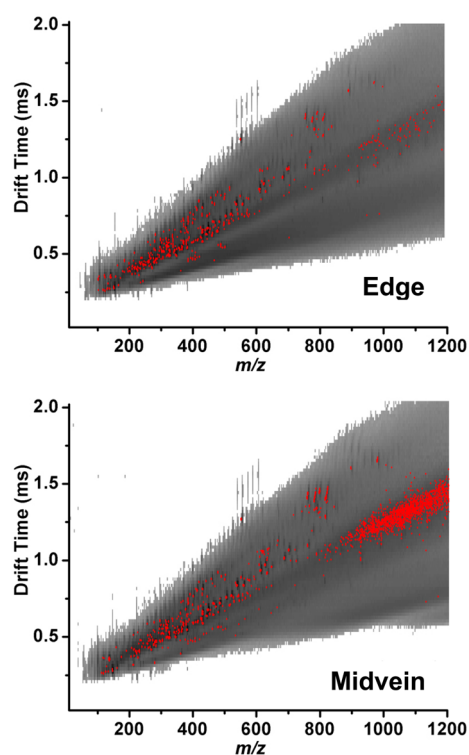
Figure 4. DT vs *m/z* plots from edge (top) and midvein (bottom) of *A. thaliana* leaves represent extensive data sets with hundreds of peaks each. Their direct manual comparison is impractical.

the corresponding peaks account for significantly more of the variance between the edge and midvein spectra.

To further explore the ion intensity differences between the DT vs *m/z* plots of the leaf edge and midvein regions, the HDMS Compare software (version 1.0, Waters, Milford, MA) was utilized. This software uses the iterative Markov chain Monte Carlo technique to achieve simultaneous peak alignment

in the DT vs *m/z* plots and to identify the statistically significant differences between the data sets.[56] Figure 5 shows the *m/z* vs DT fusion heat plots highlighting the differences between the edge and midvein data. The red color represents the areas with higher signal from the edge, whereas the blue color indicates areas with higher intensity from the midvein. The inset in the bottom right shows a zoomed portion of the heat plot focusing on the *m/z* 315−415 range, where the potassiated sucrose is found to be more prevalent in the midvein. The top right inset shows the corresponding mass spectra, where the average ion intensity for sucrose is indeed 2 times higher at the midvein than at the edge. The heat plot can be used to find numerous other differences in the DT vs *m/z* plots that can be further explored by OPLS-DA or other multivariate statistical methods.

■ CONCLUSIONS

The results presented here show the first combination of a LAESI direct ionization source with on the fly separation based on IMS followed by MS. We have demonstrated the applicability of LAESI-IMS-MS to untreated biological samples, e.g., MEG-01 cell pellets, mouse brain sections, and *A. thaliana* leaf segments, where ions are first separated based on their collision cross section then further analyzed based on their mass-to-charge ratios. These examples indicate that by employing the IMS separation step, we have improved the molecular coverage for complex samples, increased the S/N ratio for ions with chemical interferences, enhanced sensitivity, and extended selectivity for isobaric species. We have shown that in comparative analysis, DT can be used to improve multivariate statistical analysis in the search for potential biomarkers.

A significant limitation in comparative LAESI-IMS-MS studies was the excessive effort needed to identify the differences in the generated large data sets. We have shown that employing multivariate statistical analysis (e.g., OPLS-DA) and binary comparison tools (HDMS Compare) can streamline
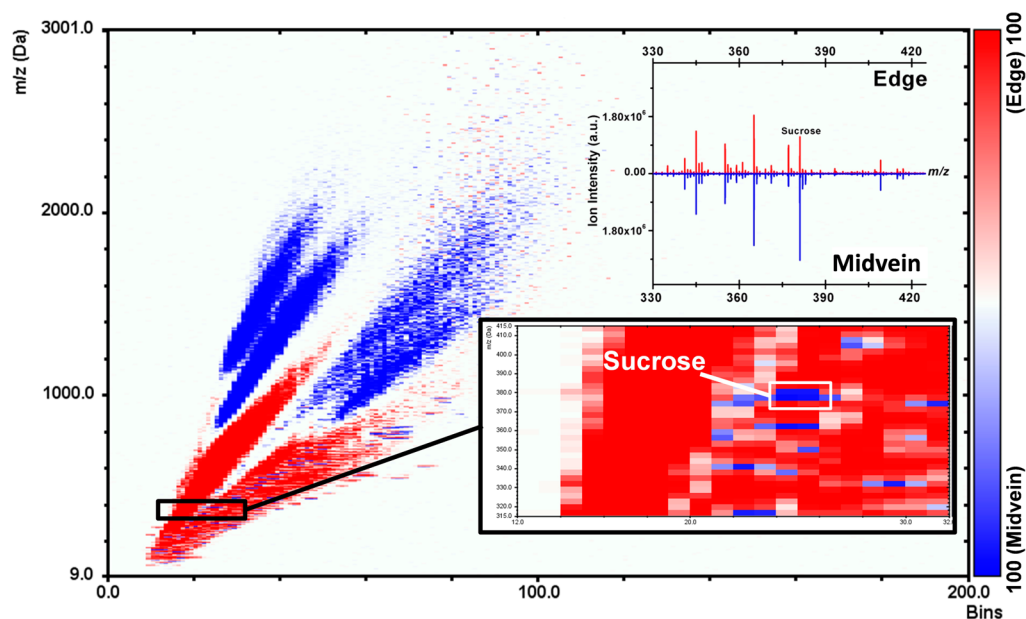

Figure 5. DT vs *m/z* heat plot shows the differences between the plots from the edge and midvein in Figure 4. The inset in the bottom right of the panel shows the area zoomed to the vicinity of potassiated sucrose ions. Corresponding mass spectra in the top right of the panel show higher intensity for these ions in the midvein spectrum.

the data analysis and help to suggest potential biomarkers. Additional tools are needed to efficiently extract information from the large data sets produced by LAESI-IMS-MS experiments.

We have also shown that LAESI-IMS-MS can be utilized to determine the collision cross sections of the detected ions and therefore facilitate their identification. In future studies, further optimization of the IMS parameters, such as the use of different drift gases, is needed to yield better separation by increasing the DT/ΔDT resolving power. In summary, LAESI-IMS-MS has shown promise for the direct analysis of complex biological samples in their native state with potential for wide-ranging biomedical utility.

■ ASSOCIATED CONTENT

Ⓢ Supporting Information
Additional information as noted in the text. This material is available free of charge via the Internet at http://pubs.acs.org.

■ AUTHOR INFORMATION

Corresponding Author
*E-mail: vertes@gwu.edu. Phone: +1 (202) 994-2717. Fax: +1 (202) 994-5873.

Notes
The authors declare no competing financial interest.

■ ACKNOWLEDGMENTS

■ REFERENCES

(1) Takáts, Z.; Wiseman, J. M.; Gologan, B.; Cooks, R. G. *Science* **2004**, *306*, 471−473.
(2) Cody, R. B.; Laramee, J. A.; Durst, H. D. *Anal. Chem.* **2005**, *77*, 2297−2302.
(3) Nemes, P.; Vertes, A. *Anal. Chem.* **2007**, *79*, 8098−8106.
(4) Nemes, P.; Vertes, A. *TrAC, Trends Anal. Chem.* **2012**, *34*, 22−33.
(5) Badu-Tawiah, A. K.; Eberlin, L. S.; Ouyang, Z.; Cooks, R. G. *Annu. Rev. Phys. Chem.* **2013**, *64*, 481−505.
(6) Monge, M. E.; Harris, G. A.; Dwivedi, P.; Fernández, F. M. *Chem. Rev.* **2013**, *113*, 2269−2308.
(7) Karasek, F. W. *Anal. Chem.* **1974**, *46*, 710A−720A.
(8) Eiceman, G. A.; Karpas, Z.; Hill, H. H. *Ion Mobility Spectrometry*, 3rd ed.; CRC Press: Boca Raton, FL, 2013; p 444.
(9) Tabrizchi, M.; Khayamian, T.; Taj, N. *Rev. Sci. Instrum.* **2000**, *71*, 2321−2328.
(10) Lubman, D. M.; Kronick, M. N. *Anal. Chem.* **1982**, *54*, 1546−1551.
(11) Baim, M. A.; Eatherton, R. L.; Hill, H. H. *Anal. Chem.* **1983**, *55*, 1761−1766.
(12) Spangler, G. E.; Roehl, J. E.; Patel, G. B.; Dorman, A. *Photoionization ion mobility spectrometer*. U.S. Patent 5,338,931, August 16, 1994.
(13) Wu, C.; Hill, H. H.; Rasulev, U. K.; Nazarov, E. G. *Anal. Chem.* **1998**, *71*, 273−278.
(14) Wu, C.; Siems, W. F.; Asbury, G. R.; Hill, H. H. *Anal. Chem.* **1998**, *70*, 4929−4938.
(15) Khayamian, T.; Jafari, M. T. *Anal. Chem.* **2007**, *79*, 3199−3205.
(16) Dong, C.; Wang, W.; Li, H. *Anal. Chem.* **2008**, *80*, 3925−3930.
(17) Creaser, C. S.; Griffiths, J. M. R.; Bramwell, C. J.; Noreen, S.; Hill, C. A.; Thomas, C. L. P. *Analyst* **2004**, *129*, 984−994.
(18) Bohrer, B. C.; Merenbloom, S. I.; Koeniger, S. L.; Hilderbrand, A. E.; Clemmer, D. E. *Annu. Rev. Anal. Chem.* **2008**, *1*, 293−327.
(19) Clemmer, D. E.; Hudgins, R. R.; Jarrold, M. F. *J. Am. Chem. Soc.* **1995**, *117*, 10141−10142.
(20) Wu, C.; Siems, W. F.; Klasmeier, J.; Hill, H. H. *Anal. Chem.* **1999**, *72*, 391−395.
(21) Dwivedi, P.; Wu, C.; Matz, L. M.; Clowers, B. H.; Siems, W. F.; Hill, H. H. *Anal. Chem.* **2006**, *78*, 8200−8206.
(22) von Helden, G.; Wyttenbach, T.; Bowers, M. T. *Int. J. Mass Spectrom. Ion Processes* **1995**, *146−147*, 349−364.
(23) Weston, D. J.; Bateman, R.; Wilson, I. D.; Wood, T. R.; Creaser, C. S. *Anal. Chem.* **2005**, *77*, 7572−7580.
(24) Myung, S.; Wiseman, J. M.; Valentine, S. J.; Takáts, Z.; Cooks, R. G.; Clemmer, D. E. *J. Phys. Chem. B* **2006**, *110*, 5045−5051.
(25) Likar, M. D.; Cheng, G.; Mahajan, N.; Zhang, Z. *J. Pharm. Biomed. Anal.* **2011**, *55*, 569−573.
(26) Sukumar, H.; Stone, J.; Nishiyama, T.; Yuan, C.; Eiceman, G. *Int. J. Ion Mobil. Spectrom.* **2011**, *14*, 51−59.
(27) Harris, G. A.; Graf, S.; Knochenmuss, R.; Fernandez, F. M. *Analyst* **2012**, *137*, 3039−3044.
(28) Shrestha, B.; Vertes, A. *Anal. Chem.* **2009**, *81*, 8265−8271.
(29) Stolee, J. A.; Shrestha, B.; Mengistu, G.; Vertes, A. *Angew. Chem., Int. Ed.* **2012**, *51*, 10386−10389.
(30) Shiea, J.; Huang, M.-Z.; Hsu, H.-J.; Lee, C.-Y.; Yuan, C.-H.; Beech, I.; Sunner, J. *Rapid Commun. Mass Spectrom.* **2005**, *19*, 3701−3704.
(31) Rezenom, Y. H.; Dong, J.; Murray, K. K. *Analyst* **2008**, *133*, 226−232.
(32) Sampson, J. S.; Muddiman, D. C. *Rapid Commun. Mass Spectrom.* **2009**, *23*, 1989−1992.
(33) Brady, J. J.; Judge, E. J.; Levis, R. J. *Rapid Commun. Mass Spectrom.* **2010**, *24*, 1659−1664.
(34) Liu, J.; Qiu, B.; Luo, H. *Rapid Commun. Mass Spectrom.* **2010**, *24*, 1365−1370.
(35) Sampson, J.; Hawkridge, A.; Muddiman, D. *J. Am. Soc. Mass Spectrom.* **2008**, *19*, 1527−1534.
(36) Sampson, J. S.; Murray, K. K.; Muddiman, D. C. *J. Am. Soc. Mass Spectrom.* **2009**, *20*, 667−673.
(37) Vaikkinen, A.; Shrestha, B.; Kauppila, T. J.; Vertes, A.; Kostiainen, R. *Anal. Chem.* **2012**, *84*, 1630−1636.
(38) Shrestha, B.; Nemes, P.; Nazarian, J.; Hathout, Y.; Hoffman, E. P.; Vertes, A. *Analyst* **2010**, *135*, 751−758.
(39) Pringle, S. D.; Giles, K.; Wildgoose, J. L.; Williams, J. P.; Slade, S. E.; Thalassinos, K.; Bateman, R. H.; Bowers, M. T.; Scrivens, J. H. *Int. J. Mass Spectrom.* **2007**, *261*, 1−12.
(40) Ogura, M.; Morishima, Y.; Ohno, R.; Kato, Y.; Hirabayashi, N.; Nagura, H.; Saito, H. *Blood* **1985**, *66*, 1384−1392.
(41) Ruotolo, B. T.; Benesch, J. L. P.; Sandercock, A. M.; Hyung, S.-J.; Robinson, C. V. *Nat. Protoc.* **2008**, *3*, 1139−1152.
(42) Clemmer, D. E.; Jarrold, M. F. *J. Mass Spectrom.* **1997**, *32*, 577−592.
(43) Nemes, P.; Goyal, S.; Vertes, A. *Anal. Chem.* **2008**, *80*, 387−395.
(44) Zaia, J.; Annan, B. S.; Biemann, K. *Rapid Commun. Mass Spectrom.* **1992**, *6*, 32−36.
(45) Valentine, S. J.; Anderson, J. G.; Ellington, A. D.; Clemmer, D. E. *J. Phys. Chem. B* **1997**, *101*, 3891−3900.
(46) Valentine, S. J.; Counterman, A. E.; Clemmer, D. E. *J. Am. Soc. Mass Spectrom.* **1997**, *8*, 954−961.
(47) Clemmer Group Cross Section Database. http://www.indiana.edu/~clemmer (accessed December 12, 2013).

(48) Li, J. W.; Taraszka, J. A.; Counterman, A. E.; Clemmer, D. E. *Int. J. Mass Spectrom.* **1999**, *185*, 37−47.

(49) Nemes, P.; Huang, H.; Vertes, A. *Phys. Chem. Chem. Phys.* **2012**, *14*, 2501−2507.

(50) Sripadi, P.; Shrestha, B.; Easley, R. L.; Carpio, L.; Kehn-Hall, K.; Chevalier, S.; Mahieux, R.; Kashanchi, F.; Vertes, A. *PLoS One* **2010**, *5*, e12590.

(51) Shrestha, B.; Sripadi, P.; Walsh, C. M.; Razunguzwa, T. T.; Powell, M. J.; Kehn-Hall, K.; Kashanchi, F.; Vertes, A. *Chem. Commun.* **2012**, *48*, 3700−3702.

(52) Fenn, L.; Kliman, M.; Mahsut, A.; Zhao, S.; McLean, J. *Anal. Bioanal. Chem.* **2009**, *394*, 235−244.

(53) Xiong, Y.; Mahmood, A.; Meng, Y. L.; Zhang, Y. L.; Zhang, Z. G.; Morris, D. C.; Chopp, M. In *Thymosins in Health and Disease II*; Goldstein, A. L., Garaci, E., Eds.; Blackwell Pub.: Boston, MA, **2012**; Vol. *1270*, pp 51−58.

(54) Shrestha, B.; Patt, J. M.; Vertes, A. *Anal. Chem.* **2011**, *83*, 2947−2955.

(55) Shrestha, B.; Javonillo, R.; Burns, J. R.; Pirger, Z.; Vertes, A. *Analyst* **2013**, *138*, 3444−3449.

(56) Benjamin, A. M.; Thompson, J. W.; Soderblom, E. J.; Geromanos, S. J.; Henao, R.; Kraus, V. B.; Moseley, M. A.; Lucas, J. E. *BMC Bioinf.* **2013**, *14*, 364.

Supporting Information for

High-Throughput Cell and Tissue Analysis with Enhanced Molecular Coverage by Laser Ablation Electrospray Ionization Mass Spectrometry Using Ion Mobility Separation

Bindesh Shrestha and Akos Vertes*

Department of Chemistry, W. M. Keck Institute for Proteomics Technology and Applications,

George Washington University, Washington, DC 20052, USA

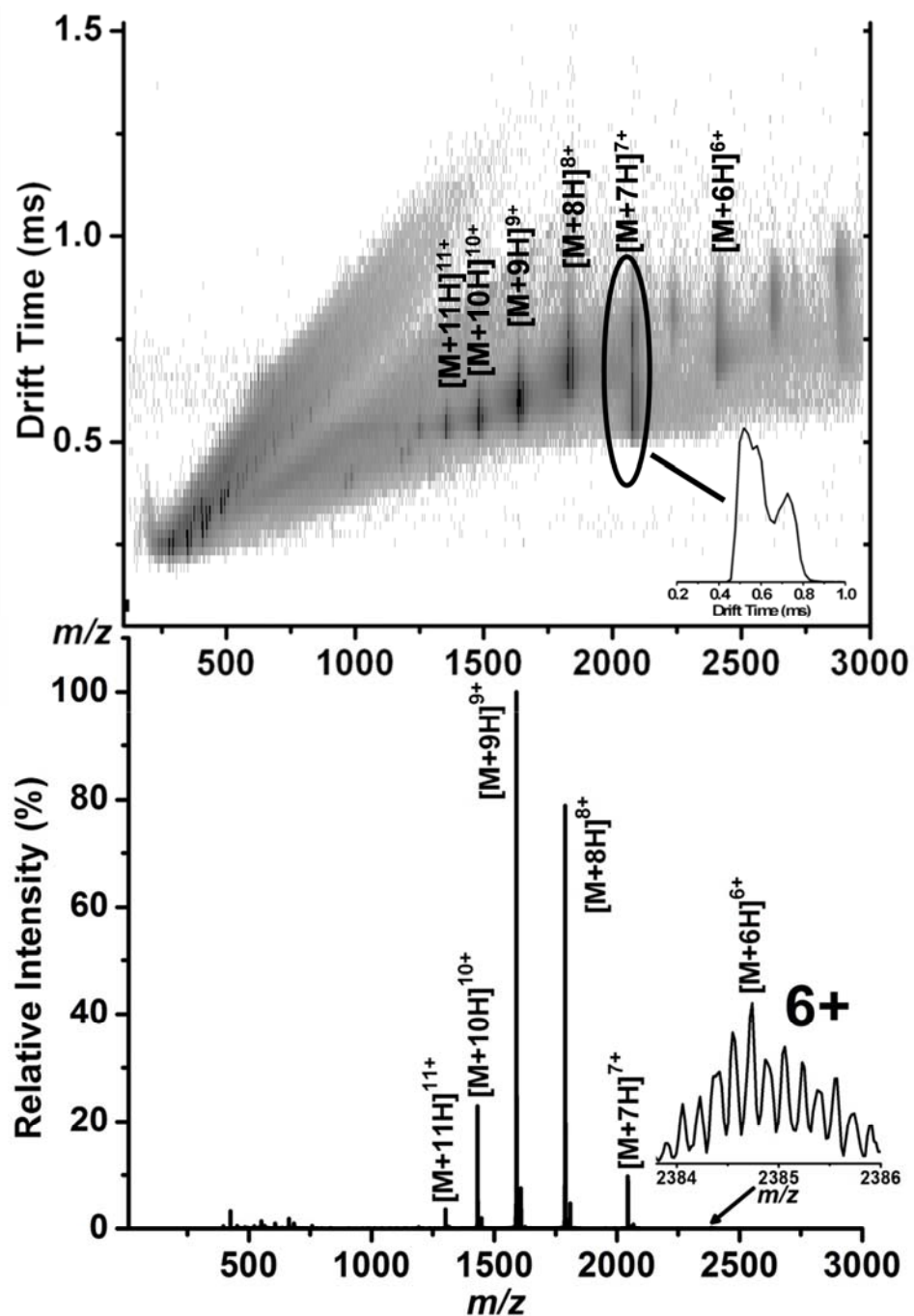*To whom correspondence should be addressed. E-mail: vertes@gwu.edu. Phone: +1 (202) 994-2717. Fax: +1 (202) 994-5873.

Figure S1a. Both DT vs. *m/z* plot and a mass spectrum of aqueous lyophilized lysozyme from chicken egg white show ions from 6+ to 11+ charge states. In the inset of DT vs. *m/z* plot, the unresolved dual peak shows intensity of $[M+7H]^{7+}$ ions across the entire drift time, which suggests presence of at least two structural conformers for that particular charge state. An example of resolved isotopic distribution of ions is presented by zooming in lowest abundance $[M+6H]^{6+}$ ion at m/z 2385.
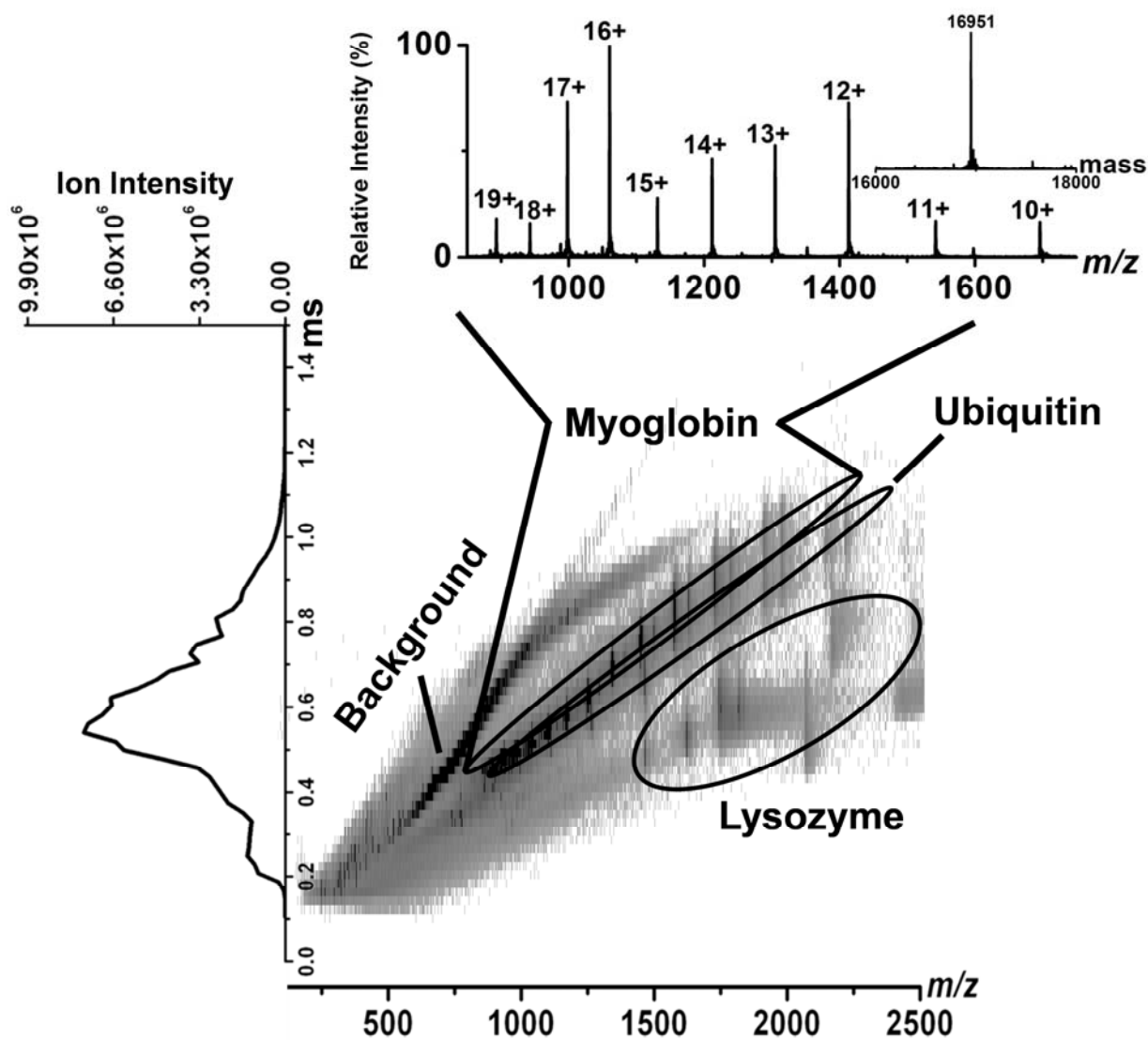
Figure S1b. DT vs. *m/z* plot of a protein mixture consisting myoglobin, ubiquitin, and lysozyme with encircled areas indicating peaks belonging to individual proteins. Drift time distribution is presented on the left. LAESI-IMS-MS spectrum integrated over the selected region for myoglobin ions is on top with the deconvoluted spectrum shown in the inset. The background ions are predominantly from impurities in lysozyme and myoglobin.
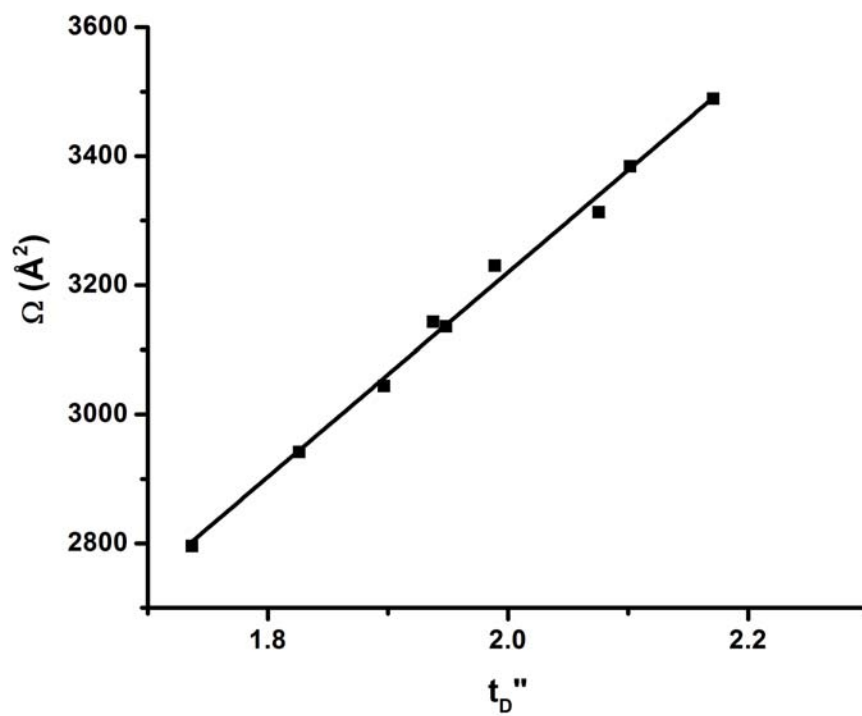
Figure S1c. Collision cross-sections for multiply protonated myoglobin species as a function of transformed corrected drift times, t_D'', follow a linear relationship.
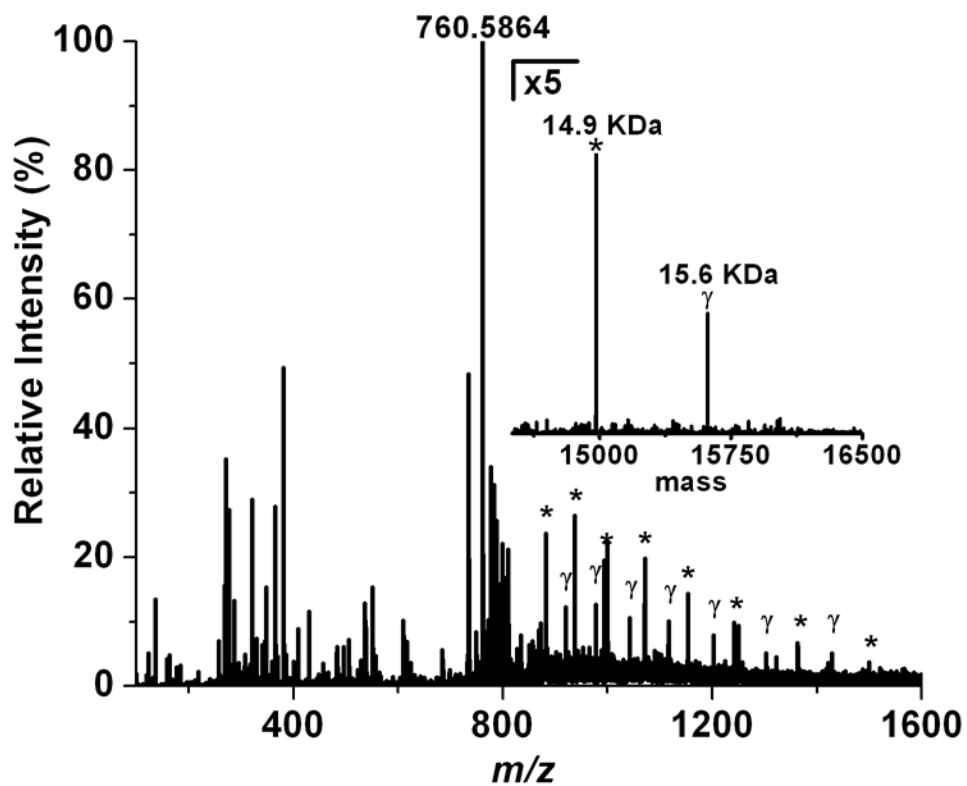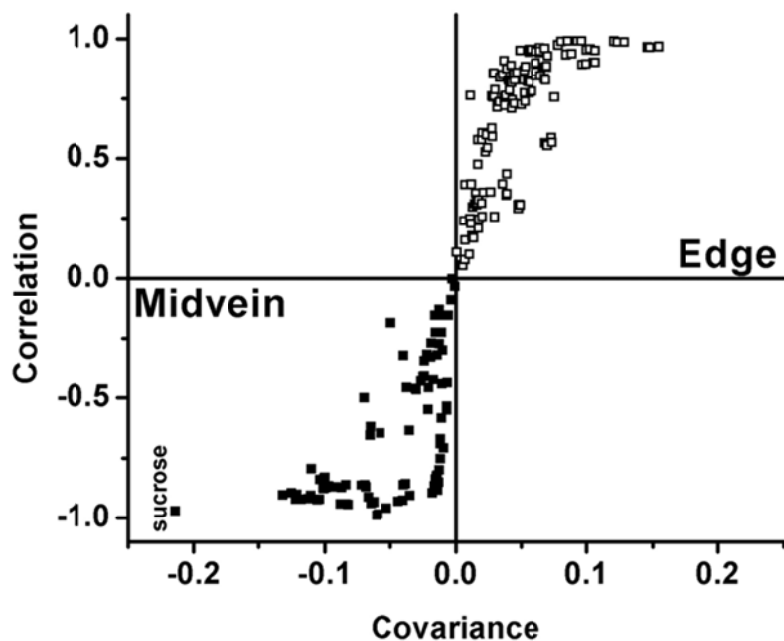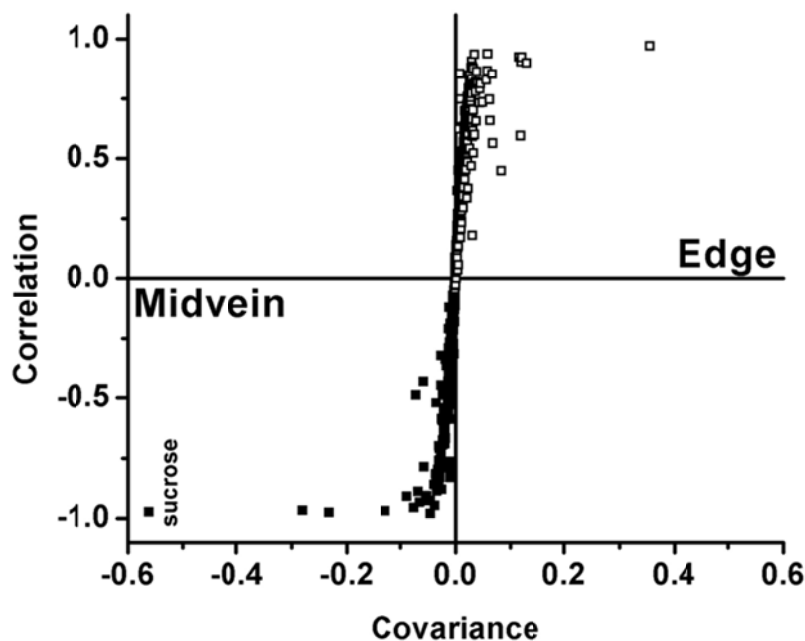
Figure S2. Mass spectrum corresponding to the protein region in the DT vs *m/z* plot show two series of multiply charged protein ions marked by * and γ. Deconvoluted spectrum in the inset of Figure 4b indicates the presence of two proteins with molecular masses of 14.9 kDa (*) and 15.6 (γ) kDa.

(a)

(b)
Figure S3. Comparative analysis of DT vs. *m/z* plots from edge and midvein, of *A. thaliana* leaves shown in Figure 5. S-plots based on the OPLS-DA model explore the variances between the two leaf sections (edge − positive axis and midvein − negative-axis). **(a)** S-plot of the entire dataset that utilized drift times to improve analysis. **(b)** S-plot at a specific drift time (DT = 0.52 ms), where the covariance between small subset of molecules present at that drift time is enhanced (see sucrose ion).

Table S1. Measured collision cross-sections of lysozyme and ubiquitin ions based on the calibration curve of myoglobin.

Protein	*m/z*	Charge state (z)	Collision cross sections ($\mathring{A}^2$)	
			*reference**	*measured*
Lysozyme	2043	7	1364	1384
			1674	1723
	1788	8	1781	1743
			2203	2249
	1590	9	1899	1827
			2384	2375
	1431	10	1961	1929
			2390	2323
Ubiquitin	1713	5	1137	1135
	1428	6	1525	1553
	1224	7	1580	1549
	1072	8	1622	1610

*Clemmer Group Cross Section Database: http://www.indiana.edu/~clemmer